

PCCP

Accepted Manuscript



This is an *Accepted Manuscript*, which has been through the Royal Society of Chemistry peer review process and has been accepted for publication.

Accepted Manuscripts are published online shortly after acceptance, before technical editing, formatting and proof reading. Using this free service, authors can make their results available to the community, in citable form, before we publish the edited article. We will replace this *Accepted Manuscript* with the edited and formatted *Advance Article* as soon as it is available.

You can find more information about *Accepted Manuscripts* in the [Information for Authors](#).

Please note that technical editing may introduce minor changes to the text and/or graphics, which may alter content. The journal's standard [Terms & Conditions](#) and the [Ethical guidelines](#) still apply. In no event shall the Royal Society of Chemistry be held responsible for any errors or omissions in this *Accepted Manuscript* or any consequences arising from the use of any information it contains.

***Ab Initio* Investigation of the Aqueous Solvation of the Nitrate Ion**

Spencer R. Pruitt,^{§,‡} Kurt R. Brorsen[‡] and Mark S. Gordon[‡]

[§] Argonne Leadership Computing Facility, Argonne, Illinois 60439, United States

[‡] Department of Chemistry, Iowa State University, Ames, Iowa 50011, United States

Abstract

The surface affinity of the nitrate ion in aqueous clusters is investigated with a variety of theoretical methods. A sampling of structures in which the nitrate ion is solvated by 32 water molecules is optimized using second order Møller-Plesset perturbation theory (MP2). Four of these MP2 optimized structures are used as starting points for fully *ab initio* molecular dynamics simulations at the dispersion corrected restricted Hartree-Fock (RHF-D) level of theory. The nitrate ion solvated by 16, 32, and 64 water molecules is also investigated with umbrella sampling molecular dynamics simulations using QM/MM methodology, where the nitrate ion is modeled with MP2 and the water molecules are described using either the non-empirical effective fragment potential (EFP) or the empirical TIP5P potential. The turning point between surface and interior solvation of the nitrate ion is predicted to lie around a cluster size of 64 water molecules.

1. Introduction

The ubiquitous water molecule has been exhaustively studied¹⁻⁷, with a great deal of effort devoted to developing many model potentials and force fields (FF)⁸⁻²⁹. However, even after decades of research, there are still areas in which the role of water is a mystery³⁰. Most commonly, the inclusion of water as a solvent is aimed at predicting bulk effects, invoking periodic boundary conditions, and involving thousands of water molecules at great

computational cost. In many cases, including a large number of water molecules in the calculation is necessary to properly describe the chemistry or biology of interest. Therefore, water is most often described using computationally inexpensive model potentials and force fields.

There are, on the other hand, many processes that involve nucleation of a solute with a cluster of only tens or hundreds of solvent molecules. These smaller systems can be treated using more accurate methods, and also provide an opportunity to benchmark model potentials against reliable quantum mechanics (QM). The small system size also allows for a comparison between FF and QM approaches for the important question of whether the nucleation chemistry of interest is more likely to occur on the surface or in the interior of the cluster. The location of the chemistry in such clusters is driven by many factors, including the surface affinity of the chemical species being solvated, the concentration of the solute(s), the temperature, and the nature and strength of the solute-solvent interactions. Furthermore, the size of the cluster plays an important role³¹, impacting the chemistry by changing the surface propensity of a given solute after a critical mass of solvent molecules has accumulated³².

Of all the aqueous-solvated ions studied, nitrate is arguably the most abundant and important. Nitrate is a highly reactive molecule³³⁻³⁵ with a role in many biological processes³⁶⁻³⁸, and nitrate is a major player in atmospheric chemistry.³⁹⁻⁴⁴ Consequently, the solvation and behavior of aqueous nitrate has been the subject of a great many experimental and theoretical research papers^{32, 41, 44-56}. The discussion of whether a variety of ions, particularly nitrate, prefer to reside on the surface or the interior of aqueous solutions has been ongoing for the better part of the last century.^{35, 57}

The focus of the present study is two-fold: (a) to investigate the surface affinity of the nitrate ion in small water clusters using highly accurate methods, and (b) to determine the efficacy of using a common model potential for describing the solvation of an important anionic molecule. Three types of *ab initio* methods were used for the investigation. The predictions of these *ab initio* methods are compared with those resulting from previous calculations^{46, 47, 58}, and from simulations carried out with a classical model potential.

2. Computational Details

2.1 *ab initio* Methods

In a previous study⁴⁶ of the surface affinity of the nitrate ion in water clusters, a variety of local minimum structures were obtained using Monte Carlo⁵⁹ simulations with simulated annealing⁶⁰ (MC/SA) to sample the potential energy surface of the nitrate ion solvated with 32 water molecules. The nitrate ion in these simulations was modeled using second order Møller-Plesset perturbation theory⁶¹ (MP2) with the DH(d,p) basis set, solvated with 32 effective fragment potential (EFP)^{23, 62} water molecules. The EFP method is an *ab initio*-based potential capable of modeling solvation using water (EFP1)²³ or a variety of organic solvents (EFP2)⁶³⁻⁶⁵. The version used in the current study (EFP1) was parameterized specifically to describe aqueous solvation effects and has been shown to be computationally efficient, as well as capable of reproducing fully *ab initio* results^{66, 67}. Single-point energy calculations on each of the clusters were performed in the previous work using MP2/DH(d,p) for the entire cluster to obtain improved relative energies of the various nitrate ion positions within the water droplet. Selected $\text{NO}_3^-(\text{H}_2\text{O})_{32}$ isomers were fully optimized with MP2/DH(d,p). The latter calculations predict that the lowest energy interior ion and surface ion structures are nearly isoenergetic.

For the present study, 30 of the previously obtained $\text{NO}_3^-(\text{H}_2\text{O})_{32}$ structures were re-optimized to determine a more accurate picture of the relative energies. Each cluster of a nitrate ion solvated with 32 water molecules was optimized with the MP2/6-31++G(d,p) level of theory. While full MP2 optimizations using this basis set were practical, Hessian calculations at the MP2 level of theory are still computationally intractable.

2.2 Fragment Molecular Orbital Molecular Dynamics

Molecular dynamics simulations of a nitrate ion solvated with 32 water molecules were also performed using the fragment molecular orbital (FMO) method. The details of the FMO method, as well as the extension of the FMO method to molecular dynamics (MD) simulations, have been discussed elsewhere^{68,69-71}, so only a brief summary is given below. An extensive review of the FMO and related methods has recently appeared⁷²⁻⁷⁶ in the literature.

2.2.1 The Fragment Molecular Orbital Method

The FMO method is based on a many-body expansion of the energy.⁷⁷ The total energy within the FMO formalism can be written as

$$E = \sum_I^N E_I + \sum_{I>J}^N (E_{IJ} - E_I - E_J) + \sum_{I>J>K}^N \{ (E_{IJK} - E_I - E_J - E_K) - (E_{IJ} - E_I - E_J) - (E_{JK} - E_J - E_K) - (E_{KI} - E_K - E_I) \} + \dots \quad (1)$$

The energy obtained from the first sum over individual fragments I (monomers) plus the second sum over fragment pairs IJ (dimers) is termed the FMO2 energy (E^{FMO2}). Inclusion of the third summation over fragment triples IJK (trimers) is termed the FMO3 energy (E^{FMO3}). At the

FMO2 level of theory, many-body effects greater than pairwise interactions are included through the use of an electrostatic potential (ESP) generated by an iterative process at the monomer level. The present paper only considers the FMO2 level of theory.

All n -mer energies are modified to account for the presence of all other fragments through incorporation of the ESP term ($V_{\mu\nu}^x$), derived from the densities of the other fragments K :

$$V_{\mu\nu}^x = \sum_{K \neq x} (u_{\mu\nu}^K + v_{\mu\nu}^K) \quad (2)$$

$$u_{\mu\nu}^K = \sum_{A \in K} \langle u | (-Z_A / |\mathbf{r} - \mathbf{r}_A|) | v \rangle \quad (3)$$

$$v_{\mu\nu}^K = \sum_{\lambda\sigma \in K} D_{\lambda\sigma}^K (\mu\nu | \lambda\sigma) \quad (4)$$

The two terms in eq. 2, $u_{\mu\nu}^K$ and $v_{\mu\nu}^K$, represent the nuclear attraction and the two-electron contributions to the energy, respectively. A number of approximations to both the ESP and far separated dimers have been implemented⁷⁸ to reduce the computational cost of the method. In conjunction with the distance-based approximations to the ESP, the energy expression in eq. 1 can be reformulated as

$$E^{FMO2} = \sum_I^N E_I^0 + \sum_{I>J}^N (E_{IJ}^0 - E_I^0 - E_J^0) + \sum_{I>J}^N Tr(\Delta\mathbf{D}^{IJ} \mathbf{V}^{IJ}) \quad (5)$$

where E_x^0 represents the internal n -mer energy with the ESP contributions subtracted out, and $\Delta\mathbf{D}^x$ is the difference density matrix defined as

$$\Delta \mathbf{D}^{IJ} = \mathbf{D}^{IJ} - \mathbf{D}^I \oplus \mathbf{D}^J \quad (6)$$

The reformulated energy expression in eq. 5 contains the contribution from the ESP to the monomer energies, indirectly through the monomer densities and directly to the dimer energies (and therefore the total energy). There are multiple advantages to this expression, including the ability to apply approximations to the monomer, dimer, and ESP calculations separately, while only requiring the dimer ESP (V^{IJ}) explicitly to calculate the total energy. This separation of the ESP term from the explicit n -mer calculations is important for the methodology outlined in section 2.2.2.

To facilitate MD simulations, fully analytic gradients for the FMO2 method have been developed^{79, 80} and have been applied to FMO-MD simulations⁶⁸.

2.2.2 Auxiliary Polarization

In order to account for the anionic nature of nitrate, FMO with auxiliary polarization (FMO/AP) was used⁸¹. The FMO/AP method employs a “dual basis set” approach that has been used elsewhere⁸²⁻⁸⁶. The first basis set (BS1) contains no diffuse functions and is used to generate the ESP. The second basis set (BS2) is larger than BS1, possibly including diffuse functions, and is used to obtain the internal energy of each n -mer. A brief description of the method includes the following steps:

1. A “gas phase” FMO calculation using BS1 is performed without the inclusion of the ESP.
2. A full FMO calculation including the ESP is performed using BS1.
3. A second “gas phase” FMO calculation (no ESP) is performed using the larger BS2 basis set.

After all three steps are complete, the total FMO/AP energy is calculated as

$$\begin{aligned}
 E &= \sum_I^N \tilde{E}_I^0 + \sum_{I>J}^N (\tilde{E}_{IJ}^0 - \tilde{E}_I^0 - \tilde{E}_J^0) + \sum_I^N \tilde{E}_I + \sum_{I>J}^N (\tilde{E}_{IJ} - \tilde{E}_I - \tilde{E}_J) - \\
 &\sum_I^N \tilde{E}_I^0 + \sum_{I>J}^N (\tilde{E}_{IJ}^0 - \tilde{E}_I^0 - \tilde{E}_J^0) \\
 &= \tilde{E}^{FMO,0} + \tilde{E}^{FMO} - \tilde{E}^{FMO,0}
 \end{aligned} \tag{7}$$

where $\tilde{E}^{FMO,0}$ is the energy obtained from step 1, \tilde{E}^{FMO} is the energy obtained from step 2, and $\tilde{E}^{FMO,0}$ is the energy obtained from step 3. One can think of $\tilde{E}^{FMO,0} - \tilde{E}^{FMO,0}$ as the basis set correction to step 1, in analogy with composite electronic structure methods. Evaluating the FMO energy in this way is analogous to the manner in which the many-body polarization is included in the effective fragment molecular orbital method (EFMO) using a polarizability-based potential^{87, 88}. The FMO/AP method is described in detail in a recent paper.⁸¹

2.2.3. FMO Computational Details

Four of the MP2/6-31++G(d,p) optimized structures were chosen as starting geometries for FMO-MD simulations (Figure 1). The nitrate ion and each water molecule were taken to be fragments, giving a total of 33 fragments in the system.

Each of the four clusters was equilibrated for 1 picosecond at a temperature of 300 K using an NVT ensemble. The Nosé-Hoover thermostat⁸⁹ was used to control the temperature. A step size of 2 femtoseconds was used in conjunction with the RATTLE constraint algorithm.⁹⁰ The internal geometry of each O-H bond was held fixed at 1.02 Å, while the H-O-H bond angle was allowed to fluctuate. After equilibration, each trajectory was run for 30 picoseconds of simulation using an NVE ensemble. A spherical boundary potential (SBP) with a force constant

of 2.0 kcal/mol was applied at a radius of 6.2 Å to maintain the solvent sphere (centered at the origin) over the course of each simulation.

All simulations were performed at the FMO2-RHF-D level of theory using the aug-cc-pVDZ basis set and auxiliary polarization was calculated using the cc-pVDZ basis set (FMO2-RHF-D/aug-cc-pVDZ/AP(cc-pVDZ)). The 2010 version (D3) of the Grimme empirical dispersion correction⁹¹ was used to capture the important dispersion interactions present in water systems. Default values for all approximations within the FMO method were used for each simulation. The average distance from the center of mass (COM) of the cluster was calculated over the course of each FMO-MD simulation. Radial distribution functions [g(r)] of the water hydrogen atoms around the nitrate oxygen atoms were also calculated for each FMO-MD simulation using the VMD program⁹².

2.3 Effective Fragment Potential Umbrella Sampling

To further investigate the surface affinity of the nitrate ion in a variety of cluster sizes, MD simulations using the NVT ensemble were performed with umbrella sampling. Cluster sizes of 16, 32, and 64 water molecules were used to solvate the nitrate ion. Each cluster size used a spherical boundary potential with a force constant of 3.0 kcal/mol/Å applied at the edge of each cluster (4.9, 6.2, and 7.8 Å from the origin, respectively) to hold the cluster centered at the origin. Umbrella sampling windows were created every 0.5 Å starting at the origin and ending at the edge of the cluster. An umbrella sampling force constant of 2.0 kcal/mol/Å was applied to the nitrate ion in each window. The total number of simulations for each cluster size of 16, 32, and 64 water molecules was 10, 13, and 16 respectively.

The nitrate in each simulation was modeled at the MP2/6-311++G(3df,2p) level of theory. Two different model potentials were used to represent the water molecules: EFP1¹⁹ and TIP5P¹⁴. Each simulation was equilibrated for 50 ps using the NVT ensemble, followed by 100 ps of production simulations at 300 K. Both equilibration and production simulations used the velocity Verlet integration with a 1.0 fs step size. The data from each set of umbrella sampling simulations was used to compute the potential of mean force (PMF) via the weighted histogram analysis method (WHAM)^{93,94}.

All calculations were performed using the General Atomic and Molecular Electronic Structure System (GAMESS).⁹⁵ Molecular visualizations for Figures 1 and 5 were generated using the UCSF Chimera program package⁹⁶.

3. Results

3.1 MP2 Optimizations

Relative energies for the 30 MP2/6-31++G(d,p) optimized $[\text{NO}_3]^{-}(\text{H}_2\text{O})_{32}$ clusters are shown in Figure 2. Interior versus surface structures are assigned based on the presence of a water molecule exterior to the nitrate ion at the cluster edge, effectively “covering up” the nitrate ion at the edge of the cluster. The lowest energy structures are predominantly those in which the nitrate ion is located near or at the surface of the cluster. One interior structure is 1.8 kcal/mol higher in energy than the lowest energy surface isomer; however, the remaining nine interior structures are between 6 and 19 kcal/mol higher in energy. This is slightly different from the previous fully optimized MP2 calculations⁴⁶ that were performed on $\text{NO}_3^{-}(\text{H}_2\text{O})_{32}$ using a smaller basis set. Those earlier calculations predicted that the lowest energy interior and surface structures were

essentially isoenergetic. On average, in the present work, the energy difference between surface and interior clusters is 11.6 kcal/mol, compared to an average of 7 kcal/mol found previously with the smaller basis set⁴⁶.

The MP2/6-31++G(d,p) optimized structures predict that the nitrate prefers to be located on the surface of a cluster of 32 water molecules. These results are in agreement with previous MP2 optimizations and show the efficacy of using the EFP method in previous work⁴⁶ for mapping the general features of the potential energy surface (PES) of solvated ions. To more accurately investigate the surface affinity of the nitrate ion, MD simulations were performed to provide a more dynamic view of the PES.

3.2 Fragment Molecular Orbital Molecular Dynamics

The four starting structures for the FMO2-RHF-D/aug-cc-pVDZ/AP(cc-pVDZ) MD simulations are shown in Figure 1. Each configuration was intentionally chosen with the nitrate near the center of the cluster. After the 30 ps of production NVE simulation time, the distance of the nitrate ion from the COM of the cluster during the simulation was calculated and plotted (Figure 3). All four simulations behaved in a similar fashion, with the nitrate ion rapidly moving from near the center of the cluster (between 0.0 and 1.8 Å), outward towards the surface of the cluster in a time averaged over all four simulations of ~ 4.5 ps. Over the course of each simulation, the nitrate ion was observed to fluctuate between ~ 4 and 6 Å from the COM of the cluster, with occasional movements outside this range towards both the interior and exterior of the cluster. The average position of the nitrate ion with respect to the center of mass of the cluster for each simulation was 4.42, 4.73, 4.59, and 4.63 Å, with a distance from the COM (averaged over all four simulations) of 4.59 Å.

These simulations showed that the nitrate ion has a strong propensity to move away rapidly from the center of a cluster of 32 water molecules. On average, the position of the nitrate ion was observed to fluctuate around a location just beneath the actual surface of the cluster, with both fully solvated and exposed structures existing over the course of the simulations. This behavior is in general agreement with the relative energies obtained from the MP2 optimized clusters, showing a stronger propensity for the surface of the cluster, while at the same time existing briefly in stable interior configurations.

To better understand the structure of the molecular cluster, RDFs of the water hydrogen atoms around the nitrate oxygen atoms were generated (Figure 4). The first solvation shell around the nitrate ions existed at ~ 1.9 Å, while the second solvation shell was calculated to be at ~ 3.4 Å. Both of these calculated values are in agreement with previously published results⁴⁶. The size of the cluster, as well as the solvation behavior around the nitrate, suggests that a cluster of 32 water molecules is not large enough to fully solvate the nitrate ion within the first solvation shell. It is possible that a minimum of two solvation shells is necessary to maintain the nitrate ion in a stable interior configuration. The ability of a larger cluster of 64 water molecules to completely solvate the nitrate ion was investigated using the validated MP2/EFP methodology.

3.3 Effective Fragment Potential Umbrella Sampling

In previous sections, the affinity of the nitrate ion to lie on or near the surface of a cluster of 32 water molecules was well established. The first solvation shell of water hydrogen atoms around the nitrate ion oxygen atoms was found to be at ~ 1.9 Å, with the second solvation shell lying at ~ 3.4 Å. In an effort to determine if a cluster of 64 water molecules would be sufficient to enclose the nitrate ion in both the first and second solvation shells, QM/MM MD simulations

were performed in conjunction with umbrella sampling to obtain the potential of mean force (PMF) for the nitrate ion solvated by clusters of 16, 32, and 64 water molecules (Figure 5). It has been established in previous work⁴⁶ that the MP2/EFP1 methodology provides a good representation of the behavior of the nitrate ion in aqueous solution. To investigate another commonly used water model, both the *ab initio* based EFP1 model potential, and the TIP5P empirical potential, were used to model the water molecules.

The PMFs generated from the umbrella sampling simulations are shown in Figure 6. The first two PMFs, Figures 6a and 6b, show the MP2/EFP behavior of the nitrate ion solvated by 16 and 32 water molecules, respectively. In each instance, the nitrate ion strongly disfavors the interior portion of the cluster, instead preferring to reside on the surface of each cluster size. However, TIP5P predicts the opposite behavior, with the nitrate ion preferring instead to be located on the interior of the cluster. Overall, the TIP5P water potential predicts complete solvation of the nitrate ion at only 16 water molecules.

Figure 6c shows the PMFs for EFP and TIP5P obtained from simulations of the nitrate ion solvated by 64 water molecules. In section 3.2, it was suggested that the cluster of 32 water molecules might not be large enough to stabilize the nitrate ion inside both the first and second solvation shells. While the PMF from the 64-water TIP5P simulations still predict a strong affinity for the interior of the cluster, the EFP simulations suggest a more ambiguous situation. The PMF begins to flatten out, exhibiting more features on the interior of the cluster in the region $\sim 2\text{-}5$ Å from the center. These stable regions correspond to the nitrate ion residing on the interior of the cluster. In the region around 2.5 Å the nitrate appears to be solvated by both the first and second solvation shells. While the overall preference of the nitrate ion is still to exist on

or near the surface of the cluster, it appears that the turning point between surface and interior for the nitrate ion begins to occur at a cluster size of 64 water molecules. This result is in contrast to previously published work⁴⁶ suggesting, based on the Amber8 force field, that the turning point occurs between 300 and 500 water molecules.

To provide a *qualitative* discussion of the observed behavior, the binding energies of $(\text{H}_2\text{O})_2$, $[\text{NO}_3]^-(\text{H}_2\text{O})$, and $[\text{NO}_3]^-(\text{H}_2\text{O})_2$ were calculated at the MP2/6-311++G(3df,2p) level of theory, neglecting temperature effects and zero point energy (ZPE) corrections. The calculated binding energy of water dimer is 5 mH, while the binding energy of the nitrate ion and a single water molecule is over five times larger (27 mH). The addition of the nitrate anion to the water dimer increases the water-water binding energy by nearly 10 mH. This local strengthening of the hydrogen bonding between water molecules due to the presence of the nitrate ion could play a role in the surface affinity of the ion.

4. Conclusions

The surface affinity of the nitrate ion was investigated with three different theoretical models: MP2 optimizations, FMO2-RHF-D/aug-cc-pVDZ/AP(cc-pVDZ) MD simulations, and MP2-EFP umbrella sampling. All three models show that at a cluster size of 32 water molecules, the nitrate ion prefers to be located at or near the surface of the cluster. According to the MP2/EFP umbrella sampling, the probability that the nitrate ion is located near the interior of the cluster, or contained in between the first and second solvation shells, increases at a cluster size of 64 water molecules. The data *suggests* that the turning point between surface and interior for the nitrate ion lies around a cluster size of 64 water molecules.

Gas phase MP2 optimizations show a slight preference for the nitrate to reside on the surface of the cluster, with low-lying interior isomers also possible. Dynamic simulations of $[\text{NO}_3]^{-}(\text{H}_2\text{O})_{32}$ show similar behavior over the 30 ps simulations, with the nitrate ion briefly residing nearer to the COM of the small cluster. It is likely that at a cluster size of 32 water molecules, the ZPE and temperature effects accounted for during dynamical simulations are large enough to push the nitrate ion to the surface of the cluster, but not strong enough to consistently break the water hydrogen bonding network. Even when located at the interior of the cluster after equilibration, all that the nitrate ion appears to need to escape the interior is a break in the hydrogen-bonding network that is large enough and long enough lived, coupled with the ZPE and temperature effects. Larger cluster sizes of 64 water molecules can create a second solvation shell around the nitrate ion, decreasing the probability of this “opening” in the hydrogen bonding network existing.

It is possible that the nitrate prefers to reside at or near the surface of the water cluster because water forms very strongly bound clusters through its three-dimensional hydrogen bonding network, thereby preventing the nitrate from easily penetrating the water cluster. The apparent local strengthening effect of the nitrate ion on the water-water interactions only makes this penetration more difficult. To properly model the three-dimensional hydrogen bonding network in water, future work will focus on the nitrate ion solvated with larger clusters sizes of up to 256 water molecules using the three-body corrected FMO method at the MP2 level of theory in an attempt to provide conclusive evidence of this behavior.

Acknowledgements

This work was supported by a U.S. National Science Foundation Software Infrastructure (SI2) grant, ACI – 1047772. The authors thank Prof. Cheol Ho Choi and Dr. Christopher Knight for many helpful discussions. Molecular graphics were generated using the UCSF Chimera package. Chimera was developed by the Resource for Biocomputing, Visualization, and Informatics at the University of California, San Francisco (supported by NIGMS P41-GM103311). Some of the computations reported here were performed on the Iowa State University Cyence cluster, obtained via a National Science Foundation MRI grant, at Iowa State University. An award of computer time was provided by the Innovative and Novel Computational Impact on Theory and Experiment (INCITE) program. This research used resources of the Argonne Leadership Computing Facility, which is a DOE Office of Science User Facility supported under Contract DE-AC02-06CH11357.

References

1. A. A. Niazi, B. D. Rabideau and A. E. Ismail, *J. Phys. Chem. B*, 2013, **117**, 1378-1388.
2. A. Nilsson, C. Huang and L. G. Pettersson, *J. Mol. Liq.*, 2012, **176**, 2-16.
3. G. Murdachaew, C. J. Mundy, G. K. Schenter, T. Laino and J. r. Hutter, *J. Phys. Chem. A*, 2011, **115**, 6046-6053.
4. J. Kim, S. B. Suh and K. S. Kim, *J. Chem. Phys.*, 1999, **111**, 10077-10087.
5. M. J. Elrod and R. J. Saykally, *Chem. Rev.*, 1994, **94**, 1975-1997.
6. F. H. Stillinger, *Theo. Chem. Adv. Pers.*, 1978, **3**, 177-234.
7. G. Bertrand, F. Millero, C. Wu and L. Hepler, *J. Phys. Chem.*, 1966, **70**, 699-706.
8. R. Skyner, J. McDonagh and C. R. Groom, *Phys. Chem. Chem. Phys.*, 2015, **17**, 6174-6191.
9. P. Florova, P. Sklenovsky, P. Banas and M. Otyepka, *J. Chem. Theor. Comp.*, 2010, **6**, 3569-3579.
10. K. M. P. Dyer, J.S.; Stell, G.; Pettitt, B.M., *Mol. Phys.*, 2009, **107**, 423-431.
11. J. L. F. Abascal, R. Garcia Fernandez, C. Vega and M. A. Carignano, *J. Chem. Phys.*, 2006, **125**, 166101-166102.
12. J. L. F. Abascal and C. Vega, *J. Chem. Phys.*, 2005, **123**, 234505-234512.
13. J. Abascal, E. Sanz, R. G. Fernandez and C. Vega, *J. Chem. Phys.*, 2005, **122**, 234511-234519.
14. S. W. Rick, *J. Chem. Phys.*, 2004, **120**, 6085-6093.
15. H. W. Horn, W. C. Swope, J. W. Pitera, J. D. Madura, T. J. Dick, G. L. Hura and T. Head-Gordon, *J. Chem. Phys.*, 2004, **120**, 9665-9678.
16. H. Nada and J. P. J. M. van der Eerden, *J. Chem. Phys.*, 2003, **118**, 7401-7413.
17. G. Lamoureux, A. D. MacKerell and B. Roux, *J. Chem. Phys.*, 2003, **119**, 5185-5197.
18. P. Mark and L. Nilsson, *J. Phys. Chem. A*, 2001, **105**, 9954-9960.
19. M. S. Gordon, M. A. Freitag, P. Bandyopadhyay, J. H. Jensen, V. Kairys and W. J. Stevens, *J. Phys. Chem. A*, 2001, **105**, 293-307.
20. M. W. Mahoney and W. L. Jorgensen, *J. Chem. Phys.*, 2000, **112**, 8910-8922.

21. K. Silverstein, A. Haymet and K. A. Dill, *J. Amer. Chem. Soc.*, 1998, **120**, 3166-3175.
22. A. D. MacKerell, D. Bashford, M. Bellott, R. L. Dunbrack, J. D. Evanseck, M. J. Field, S. Fischer, J. Gao, H. Guo, S. Ha, D. Joseph-McCarthy, L. Kuchnir, K. Kuczera, F. Lau, C. Mattos, S. Michnick, T. Ngo, D. T. Nguyen, B. Prodhom, W. E. Reiher, B. Roux, M. Schlenkrich, J. C. Smith, R. Stote, J. Straub, M. Watanabe, J. Wiorkiewicz-Kuczera, D. Yin and M. Karplus, *J. Phys. Chem. B*, 1998, **102**, 3586-3616.
23. P. N. Day, J. H. Jensen, M. S. Gordon, S. P. Webb, W. J. Stevens, M. Krauss, D. Garmer, H. Basch and D. Cohen, *J. Chem. Phys.*, 1996, **105**, 1968-1986.
24. M. P. A. a. D. J. Tildesley, *Computer Simulation of Liquids*, Oxford University Press, Oxford, 1989.
25. H. Berendsen, J. R. Grigera and T. P. Straatsma, *J. Phys. Chem.*, 1987, **91**, 6269-6271.
26. K. Toukan and A. Rahman, *Phys. Rev. B*, 1985, **31**, 2643-2648.
27. W. L. Jorgensen, J. Chandrasekhar, J. D. Madura, R. W. Impey and M. L. Klein, *J. Chem. Phys.*, 1983, **79**, 926-935.
28. W. L. Jorgensen, *J. Chem. Phys.*, 1982, **77**, 4156-4163.
29. F. H. Stilling and A. Rahman, *J. Chem. Phys.*, 1974, **60**, 1545-1557.
30. P. Ball, *Nat.*, 2008, **452**, 291-292.
31. S. J. Stuart and B. J. Berne, *J. Phys. Chem. A*, 1999, **103**, 10300-10307.
32. P. Jungwirth and D. J. Tobias, *J. Phys. Chem. B*, 2002, **106**, 6361-6373.
33. O. Svoboda, L. Kubelová and P. Slavíček, *J. Phys. Chem. A*, 2013, **117**, 12868-12877.
34. J. C. Fanning, *Coordination Chemistry Reviews*, 2000, **199**, 159-179.
35. J. Mack and J. R. Bolton, *Journal of Photochemistry and Photobiology A: Chemistry*, 1999, **128**, 1-13.
36. M. T. G. Jon O Lundberg, Amrita Ahluwalia, Nigel Benjamin, Nathan S Bryan, Anthony Butler, A. F. Pedro Cabrales, Martin Feelisch, Peter C Ford, Bruce A Freeman, Michael Frenneaux, Joel Friedman, Malte Kelm, Christopher G Kevil, Daniel B Kim-Shapiro, Andrey V Kozlov, Jack R Lancaster Jr, David J Lefer, Kenneth McColl, Kenneth McCurry, Rakesh P Patel, Joel Petersson, Tienush Rassaf, Valentin P Reutov, and A. S. George B Richter-Addo, Sruti Shiva, Koichiro Tsuchiya, Ernst E van Faassen, Andrew J Webb, Brian S Zuckerbraun, Jay L Zweier & Eddie Weitzberg, *Nat. Chem. Bio.*, 2009, **5**, 865-869.
37. R. J. P. Williams, *Bio-inorganic Chemistry*, American Chemical Society, Washington, DC, 1971.

38. H. Frank, *Chemical Physics of Ionic Solutions*, John Wiley & Sons, New York, 1956.
39. S.-J. Yuan, J.-J. Chen, Z.-Q. Lin, W.-W. Li, G.-P. Sheng and H.-Q. Yu, *Nature Communications*, 2014, **4**, 1-7.
40. M. G. H. B. Alexander, D.J. Allman, J. Dachs, J.A. Hornton, and S.A. Kunasek, *Atmo. Chem. Phys.*, 2009, **9**, 5043-5056.
41. P. Jungwirth and D. J. Tobias, *J. Phys. Chem. B*, 2001, **105**, 10468-10472.
42. B. J. F.-P. a. J. N. Pitts, *Chemistry of the Upper and Lower Atmosphere*, Academic, San Diego, 2000.
43. R. P. Wayne, *Chemistry of Atmospheres*, Oxford University Press, Oxford, 2000.
44. E. M. Knipping, M. J. Lakin, K. L. Foster, P. Jungwirth, D. J. Tobias, R. B. Gerber, D. Dabdub and B. J. Finlayson-Pitts, *Science*, 2000, **288**, 301-306.
45. M. Ahmed, V. Namboodiri, A. K. Singh, J. A. Mondal and S. K. Sarkar, *The journal of physical chemistry. B*, 2013, **117**, 16479-16485.
46. Y. Miller, J. L. Thomas, D. D. Kemp, B. J. Finlayson-Pitts, M. S. Gordon, D. J. Tobias and R. B. Gerber, *J. Phys. Chem. A*, 2009, **113**, 12805-12814.
47. A. Tongraar, P. Tangkawanwanit and B. M. Rode, *J. Phys. Chem. A*, 2006, **110**, 12918-12926.
48. L. X. Dang, T.-M. Chang, M. Roeselova, B. C. Garrett and D. J. Tobias, *J. Chem. Phys.*, 2006, **124**, 66101-66103.
49. A. Wahab, S. Mahiuddin, G. Hefter, W. Kunz, B. Minofar and P. Jungwirth, *J. Phys. Chem. B*, 2005, **109**, 24108-24120.
50. P. Salvador, J. E. Curtis, D. J. Tobias and P. Jungwirth, *Phys. Chem. Chem. Phys.*, 2003, **5**, 3752-3757.
51. C. Ebner, R. Sansone, S. Hengrasmee and M. Probst, *Int. J. Quant. Chem.*, 1999, **75**, 805-814.
52. Y. Ikushima, N. Saito and M. Arai, *J. Phys. Chem. B*, 1998, **102**, 3029-3035.
53. A. Laaksonen and H. Kovacs, *Can. J. Chem.*, 1994, **72**, 2278-2285.
54. H. Ohtaki and T. Radnai, *Chem. Rev.*, 1993, **93**, 1157-1204.
55. Y. Kataoka, *Bull. Chem. Soc. Jap.*, 1993, **66**, 2478-2491.
56. P. Guilbaud and G. Wipff, *J. Phys. Chem.*, 1993, **97**, 5685-5692.

57. A. R. Davis, *J Chem Phys*, 1969, **50**, 1478-1479.
58. J. Thøgersen, J. Réhault, M. Odelius, T. Ogden, N. K. Jena, S. J. K. Jensen, S. R. Keiding and J. Helbing, *J. Phys. Chem. B*, 2013, **117**, 3376-3388.
59. N. Metropolis, A. W. Rosenbluth, M. N. Rosenbluth, A. H. Teller and E. Teller, *J. Chem. Phys.*, 1953, **21**, 1087-1092.
60. S. Kirkpatrick, C. D. Gelatt and M. P. Vecchi, *Science*, 1983, **220**, 671-680.
61. C. Møller and M. S. Plesset, *Phys. Rev.*, 1934, **46**, 618-622.
62. M. S. Gordon, M. A. Freitag and P. Bandyopadhyay, *The Journal of Physical Chemistry A*, 2001, **105**, 293-307.
63. M. S. S. Gordon, L.; Li, H.; Jensen, J. H., in *Annu. Rep. Comput. Chem.*, ed. D. S. a. R. Wheeler, Elsevier B.V.2007, vol. 3, ch. 10, pp. 177-191.
64. M. S. Gordon, J. M. Mullin, S. R. Pruitt, L. B. Roskop, L. V. Slipchenko and J. A. Boatz, *The journal of physical chemistry. B*, 2009, **113**, 9646-9663.
65. D. K. Ghosh, D.; Vanovschi, V.; Williams, C. F.; Herbert, J. M.; Gordon, M. S.; Schmidt, M. W.; Slipchenko, L. V.; and A. I. Krylov, *J. Phys. Chem. A*, 2010, **114**, 12739-12754.
66. P. N. Day, R. Pachter, M. S. Gordon and G. N. Merrill, *J. Chem. Phys.*, 2000, **112**, 2063-2073.
67. G. N. Merrill and M. S. Gordon, *The Journal of Physical Chemistry A*, 1998, **102**, 2650-2657.
68. K. R. Brorsen, N. Minezawa, F. Xu, T. L. Windus and M. S. Gordon, *J. Chem. Theor. Comp.*, 2012, **8**, 5008-5012.
69. D. G. Fedorov and K. Kitaura, *The Journal of Physical Chemistry A*, 2007, **111**, 6904-6914.
70. Y. Komeiji, T. Nakano, K. Fukuzawa, Y. Ueno, Y. Inadomi, T. Nemoto, M. Uebayasi, D. G. Fedorov and K. Kitaura, *Chem. Phys. Lett.*, 2003, **372**, 342-347.
71. Y. Komeiji, Y. Mochizuki, T. Nakano and D. G. Fedorov, *Journal of Molecular Structure: THEOCHEM*, 2009, **898**, 2-7.
72. M. S. Gordon, D. G. Fedorov, S. R. Pruitt and L. V. Slipchenko, *Chem. Rev.*, 2012, **112**, 632-672.
73. D. G. Fedorov, T. Nagata and K. Kitaura, *Phys. Chem. Chem. Phys.*, 2012, **14**, 7562-7577.

74. T. Nagata, D. G. Fedorov and K. Kitaura, in *Linear-Scaling Techniques in Computational Chemistry and Physics*, Springer, Springer edn., 2011, pp. 17-64.
75. M. S. Gordon, J. M. Mullin, S. R. Pruitt, L. B. Roskop, L. V. Slipchenko and J. A. Boatz, *J. Phys. Chem. B*, 2009, **113**, 9646-9663.
76. D. G. Fedorov and K. Kitaura, *J. Phys. Chem. A*, 2007, **111**, 6904-6914.
77. D. G. Fedorov, N. Asada, I. Nakanishi and K. Kitaura, *Acc. Chem. Res.*, 2014, **47**, 2846-2856.
78. T. Nakano, T. Kaminuma, T. Sato, K. Fukuzawa, Y. Akiyama, M. Uebayasi and K. Kitaura, *Chem. Phys. Lett.*, 2002, **351**, 475-480.
79. T. Nagata, D. G. Fedorov, K. Ishimura and K. Kitaura, *J. Chem. Phys.*, 2011, **135**, 044110-044115.
80. T. Nagata, K. Brorsen, D. G. Fedorov, K. Kitaura and M. S. Gordon, *J. Chem. Phys.*, 2011, **134**, 124115-124113.
81. D. G. Fedorov and K. Kitaura, *Chem. Phys. Lett.*, 2014, **597**, 99-105.
82. R. P. Steele, M. Head-Gordon and J. C. Tully, *J. Phys. Chem. A*, 2010, **114**, 11853-11860.
83. M. Kobayashi, H. Nakai, S. Hirata, Y. Ishikawa and T. Nakajima, *Int. J. Quant. Chem.*, 2009, **109**, 2227-2237.
84. R. P. Steele, Y. Shao, R. A. DiStasio and M. Head-Gordon, *J. Phys. Chem. A*, 2006, **110**, 13915-13922.
85. K. Wolinski and P. Pulay, *J. Chem. Phys.*, 2003, **118**, 9497-9503.
86. S. Havriliak and H. F. King, *J. Amer. Chem. Soc.*, 1983, **105**, 4-12.
87. C. Steinmann, D. G. Fedorov and J. H. Jensen, *J. Phys. Chem. A*, 2010, **114**, 8705-8712.
88. S. R. Pruitt, C. Steinmann, J. H. Jensen and M. S. Gordon, *J. Chem. Theor. Comp.*, 2013, **9**, 2235-2249.
89. S. C. Harvey and R. Tan, *J. Comp. Chem.*, 1998, **19**, 726-740.
90. H. C. Andersen, *J. Comp. Phys.*, 1983, **52**, 24-34.
91. S. Grimme, J. Antony, S. Ehrlich and H. Krieg, *J. Chem. Phys.*, 2010, **132**, 154104.
92. W. D. Humphrey, A. and Schulten, K., *J. Mol. Graph.*, 1996, **14**, 33-38.

93. S. R. Kumar, J.M.; Bouzida, D.; Swendsen R.H.; Kollman, P.A., *Journal of Computational Chemistry*, 1992, **13**, 1011-1021.
94. A. Grossfield, 2.0.9 edn.
95. M. W. Schmidt, K. K. Baldrige, J. A. Boatz, S. T. Elbert, M. S. Gordon, J. H. Jensen, S. Koseki, N. Matsunaga, K. A. Nguyen, S. Su, T. L. Windus, M. Dupuis and J. A. M. Jr, *J. Comp. Chem.*, 1993, **14**, 1347-1363.
96. E. F. Pettersen, T. D. Goddard, C. C. Huang, G. S. Couch, D. M. Greenblatt, E. C. Meng and T. E. Ferrin, *J. Comp. Chem.*, 2004, **25**, 1605-1612.

Figure 1. Starting geometries for FMO2-RHF-D/aug-cc-pVDZ/AP(cc-pVDZ) molecular dynamics simulations of 4 $[\text{NO}_3]^{-}(\text{H}_2\text{O})_{32}$ clusters.

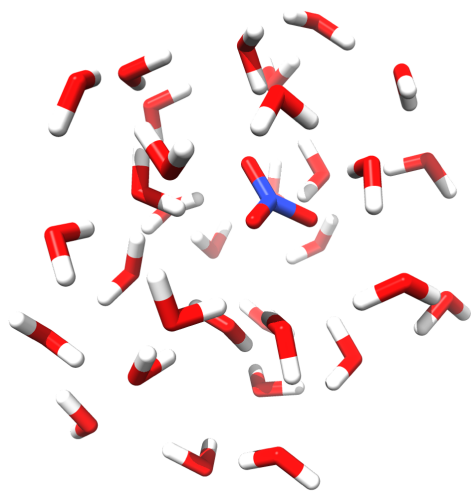
Figure 2. Relative energies of 30 $[\text{NO}_3]^{-}(\text{H}_2\text{O})_{32}$ clusters optimized at the MP2/6-31++G(d,p) level of theory. Red markers indicate structures where the nitrate is located in the interior of the cluster.

Figure 3. Distance of the nitrate molecule from the center of mass of the $[\text{NO}_3]^{-}(\text{H}_2\text{O})_{32}$ cluster for each FMO-MD simulation.

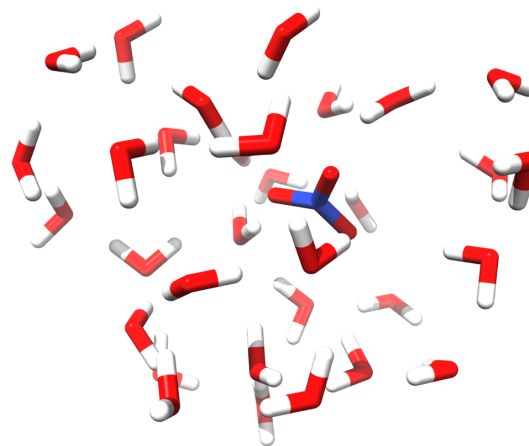
Figure 4. Radial distribution functions of the water H atoms around the nitrate O atoms, generated for each of the four FMO-MD simulations.

Figure 5. Snapshots of the most favorable geometry for each cluster size ($[\text{NO}_3]^{-}(\text{H}_2\text{O})_{16}$, $[\text{NO}_3]^{-}(\text{H}_2\text{O})_{32}$, and $[\text{NO}_3]^{-}(\text{H}_2\text{O})_{64}$) of the EFP umbrella sampling simulations.

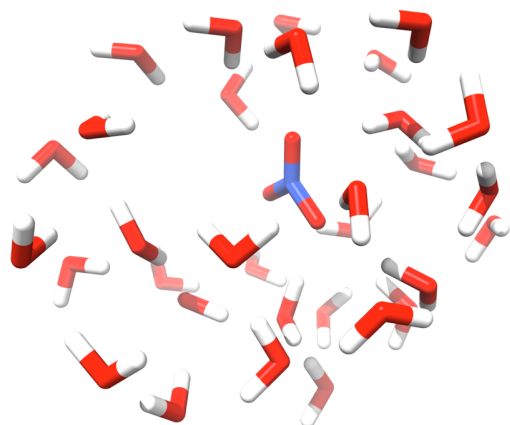
Figure 6. Potential of mean force (PMF) graphs generated for each EFP umbrella sampling simulation. The abscissa of each graph is in kcal/mol, while the ordinate is in angstroms and measured as the distance from the origin.



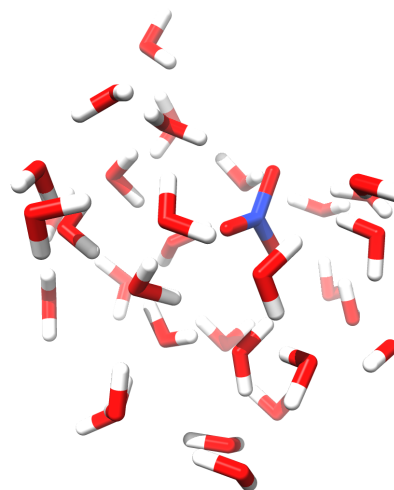
Trj 1



Trj 2



Trj 3



Trj 4

